

**Probabilistic & Reliability-based Health Monitoring Strategies for High-Speed Naval Vessels**  
Office of Naval Research (ONR) Contract Number:  
N00014-09-1-0567

**FINAL REPORT**

**Jerome P. Lynch, Ph.D., University of Michigan (PI)**  
**Kincho H. Law, Ph.D., Stanford University (Co-PI)**  
**Sean O'Connor, University of Michigan**

**Date of Report:**  
January 1, 2012

**Points of Contact:**

Jerome P. Lynch, Ph.D.  
Associate Professor  
Department of Civil and Environmental  
Engineering  
Department of Electrical Engineering and  
Computer Science  
2380 G. G. Brown Building  
Ann Arbor, MI 48109-2125  
(734) 615-5290  
jerlynch@umich.edu

Kincho H. Law, PhD  
Professor  
Department of Civil and Environmental  
Engineering  
Room 277A, Y2E2 Building  
473 Via Ortega  
Stanford University  
Stanford, CA 94305-4020  
(650) 725-3154  
[law@stanford.edu](mailto:law@stanford.edu)

DTIC<sup>®</sup> has determined on 3 / 19 / 12 that this Technical Document has the Distribution Statement checked below. The current distribution for this document can be found in the DTIC<sup>®</sup> Technical Report Database.

**DISTRIBUTION STATEMENT A.** Approved for public release; distribution is unlimited.

**© COPYRIGHTED.** U.S. Government or Federal Rights License. All other rights and uses except those permitted by copyright law are reserved by the copyright owner.

**DISTRIBUTION STATEMENT B.** Distribution authorized to U.S. Government agencies only (fill in reason) (date of determination). Other requests for this document shall be referred to (insert controlling DoD office).

**DISTRIBUTION STATEMENT C.** Distribution authorized to U.S. Government Agencies and their contractors (fill in reason) (date determination). Other requests for this document shall be referred to (insert controlling DoD office).

**DISTRIBUTION STATEMENT D.** Distribution authorized to the Department of Defense and U.S. DoD contractors only (fill in reason) (date of determination). Other requests shall be referred to (insert controlling DoD office).

**DISTRIBUTION STATEMENT E.** Distribution authorized to DoD Components only (fill in reason) (date of determination). Other requests shall be referred to (insert controlling DoD office).

**DISTRIBUTION STATEMENT F.** Further dissemination only as directed by (insert controlling DoD office) (date of determination) or higher DoD authority.

*Distribution Statement F is also used when a document does not contain a distribution statement and no distribution statement can be determined.*

**DISTRIBUTION STATEMENT X.** Distribution authorized to U.S. Government Agencies and private individuals or enterprises eligible to obtain export-controlled technical data in accordance with DoDD 5230.25; (date of determination). DoD Controlling Office is (insert controlling DoD office).

**REPORT DOCUMENTATION PAGE**

Form Approved  
OMB No. 0704-0188

The public reporting burden for this collection of information is estimated to average 1 hour per response, including the time for reviewing instructions, searching existing data sources, gathering and maintaining the data needed, and completing and reviewing the collection of information. Send comments regarding this burden estimate or any other aspect of this collection of information, including suggestions for reducing the burden, to Department of Defense, Washington Headquarters Services, Directorate for Information Operations and Reports (0704-0188), 1215 Jefferson Davis Highway, Suite 1204, Arlington, VA 22202-4302. Respondents should be aware that notwithstanding any other provision of law, no person shall be subject to any penalty for failing to comply with a collection of information if it does not display a currently valid OMB control number.

**PLEASE DO NOT RETURN YOUR FORM TO THE ABOVE ADDRESS.**

<b>1. REPORT DATE (DD-MM-YYYY)</b> 1-01-2012		<b>2. REPORT TYPE</b> Final Technical Report		<b>3. DATES COVERED (From - To)</b> April 1, 2009 - March 1, 2010	
<b>4. TITLE AND SUBTITLE</b> Probabilistic & Reliability-based Health Monitoring Strategies for High-Speed Naval Vessels				<b>5a. CONTRACT NUMBER</b> N00014-09-1-0567	
				<b>5b. GRANT NUMBER</b>	
				<b>5c. PROGRAM ELEMENT NUMBER</b>	
<b>6. AUTHOR(S)</b> Jerome P. Lynch, Ph.D. Kincho H. Law, Ph.D. Sean O'Connor				<b>5d. PROJECT NUMBER</b>	
				<b>5e. TASK NUMBER</b>	
				<b>5f. WORK UNIT NUMBER</b>	
<b>7. PERFORMING ORGANIZATION NAME(S) AND ADDRESS(ES)</b> University of Michigan 2380 G G Brown Building Ann Arbor, MI 48109-2125				<b>8. PERFORMING ORGANIZATION REPORT NUMBER</b>	
<b>9. SPONSORING/MONITORING AGENCY NAME(S) AND ADDRESS(ES)</b> Office of Naval Research Attn: Paul Hess 875 North Randolph Street Arlington, VA 22203-1995				<b>10. SPONSOR/MONITOR'S ACRONYM(S)</b> ONR	
				<b>11. SPONSOR/MONITOR'S REPORT NUMBER(S)</b>	
<b>12. DISTRIBUTION/AVAILABILITY STATEMENT</b>					
<b>13. SUPPLEMENTARY NOTES</b>  20120305031					
<b>14. ABSTRACT</b> In this project, a strategy is proposed for fatigue life estimation of a ship hull using a wireless sensor network installed in the hull for autonomous health monitoring. First, a rainflow counting algorithm is implemented as a continuous time-domain approach to fatigue estimation. Cycles are defined by a rainflow counting procedure and are kept on-board the wireless sensing unit in a histogram structure for long-term storage. Fatigue damage is accumulated by the Palmgren-Miner linear summation method. Second, a statistical approach called the Dirlik procedure is used which relies on spectral moments of the stress-time history power spectral density (PSD) function. The Dirlik procedure outputs a probability density function (PDF) of stress ranges, tailored to resemble the rainflow counting results. The PDF is converted to damage using an S-N curve and again accumulated by the Palmgren-Miner method. Experimental tests are conducted on an aluminum hull stiffened element specimen as part of the Monitored Aluminum Hull Integrity (MAHI) test program to verify the embedded fatigue life estimation procedures.					
<b>15. SUBJECT TERMS</b>					
<b>16. SECURITY CLASSIFICATION OF:</b>			<b>17. LIMITATION OF ABSTRACT</b>	<b>18. NUMBER OF PAGES</b>	<b>19a. NAME OF RESPONSIBLE PERSON</b> Jerome P. Lynch, Ph.D.
a. REPORT	b. ABSTRACT	c. THIS PAGE			<b>19b. TELEPHONE NUMBER (include area code)</b> 734-615-5290

## Table of Contents

Executive Summary .....	3
Acknowledgement .....	4
1. Introduction .....	5
2. Technical Objectives .....	5
3. Theoretical Background and Algorithms .....	6
3.1. Rain Flow Peak Extraction and Miner's Rule for Fatigue Estimation .....	6
3.2. Spectral Methods for Fatigue Estimation .....	10
4. Experimental Validation of the Embedded Fatigue Estimation Algorithms .....	13
4.1. Implementation in the <i>Narada</i> Wireless Sensor Node .....	13
4.2. Aluminum Bar Specimens under Uniaxial Tensile Loading .....	16
4.3. Validation on the Monitored Aluminum Hull Integrity (MAHI) Phase I Specimen .....	21
5. Summary and Future Direction .....	26
References .....	27

## Executive Summary

As the U.S. Navy aggressively pursues the design of high-speed aluminum vessels for littoral combat operations, there is a growing need for on-board hull monitoring systems capable of detecting hull deterioration and damage. In particular, fatigue damage is anticipated due to the combination of non-traditional hull forms and demanding seaway loads. Fatigue is an accumulated degradation process that occurs under cyclic loading, eventually inducing cracking at stress concentration points. In this project, a strategy is proposed for fatigue life estimation of a ship hull using a wireless sensor network installed in the hull for autonomous health monitoring. Specifically, the computation and storage capabilities of each wireless sensing unit are leveraged to process large, continuous amounts of raw strain gage data for fatigue life information, thereby presenting the user with very little data, yet very meaningful decision making information. First, a rainflow counting algorithm is implemented as a continuous time-domain approach to fatigue estimation. A peak picking algorithm reduces time history data to a minimum set of data points that are needed for fatigue analysis. Cycles are defined by a rainflow counting procedure and are kept on-board the wireless sensing unit in a histogram structure for long-term storage. Fatigue damage is accumulated by the Palmgren-Miner linear summation method. Second, a statistical approach called the Dirlik procedure is used which relies on spectral moments of the stress-time history power spectral density (PSD) function. The main motivation for this approach is to use a few statistical parameters from the power spectrum to estimate fatigue life rather than doing the continuous collecting and processing that is conducted in the rainflow procedure. The Dirlik procedure outputs a probability density function (PDF) of stress ranges, tailored to resemble the rainflow counting results. The PDF is converted to damage using an S-N curve and again accumulated by the Palmgren-Miner method. Damage results are kept on-board for long-term storage awaiting user query. Communication of results is done only by request, dramatically reducing the power consumption in the wireless sensing network.

Experimental tests are conducted on an aluminum hull stiffened element specimen as part of the Monitored Aluminum Hull Integrity (MAHI) test program to verify the embedded fatigue life estimation procedures. Testing is carried out at the Naval Surface Warfare Center-Carderock Division (NSWCCD) Fatigue Testing Laboratory. Among the key objectives of the MAHI test program is the demonstration and evaluation of SHM technologies. A tethered strain gage monitoring system with 16 channels is employed for laboratory data collection. A network of *Narada* wireless sensor units is used to collect multiple strain gage channels performing continuous data collection as well as the embedded rainflow and Dirlik fatigue estimation procedures. Strong agreement is found between the *Narada* and NSWCCD data. Furthermore, the accuracy of the embedded fatigue estimation algorithms is confirmed.

**Acknowledgement**

The authors would like to acknowledge the support offered by the Office of Naval Research under Contract Number N00014-09-1-0567 and N00014-10-1-0613 awarded to University of Michigan and N00014-10-1-0384 awarded to Stanford University. The authors also would like to thank Dr. Liming W. Salvino of ONR Global and Edward Devine of Naval Surface Warfare Center (NSWC) - Carderock Division for their contributions to this research. In addition, active collaborations and guidance on aluminum naval ship structures from Thomas Brady and David Kihl of the Naval Surface Warfare Center - Carderock Division are very much appreciated. Last but not least, the advice and suggestions offered by Dr. Paul Hess of ONR throughout the project are gratefully acknowledged.

## 1. Introduction

In recent years, the need for high-speed littoral combat ships (LCS) has driven U.S. Navy interest in aluminum hulls of unconventional design (e.g., multi-hull catamaran style ships). For example, the Joint High-Speed Vehicle (JHSV) and Littoral Combat Ship (LCS) programs are examples of major ship design and procurement programs instituted by the U.S. Navy (Hess 2007). While aluminum allows the ship weight to be dramatically reduced as compared to the use of steel, aluminum introduces a number of significant challenges for long-term ship operation and management (O&M). Foremost among those concerns is fatigue cracking in the aluminum hull. Fatigue is predicted to be a serious O&M issue due to a general lack of design and analytical methods for aluminum hulls, especially hulls that will experience the excessive seaway loads anticipated for LCS (Tveiten, *et al.* 2007). Since the mid-1950's, the Navy has utilized aluminum in the design and construction of the deckhouses of their steel destroyer-class ships (Sielski 2007). However, fatigue issues have emerged with these deckhouses, especially the rate of growth of fatigue cracks resulting in severe deckhouse damage in extreme sea conditions. As the Navy moves toward aluminum for the construction of LCS hulls, it is interested in the adoption of long-term hull monitoring systems that can closely monitor hull responses to seaway loads. The benefits of hull monitoring are enormous. First, hull response data can be used to validate design assumptions leading to improvements in the design of future vessels. Second, hull response data would be integral to the health assessment of the ship (*i.e.*, structural health monitoring (SHM)) and guide O&M decision making of the port engineer. The early detection of hull damage and/or deterioration allows the Navy to resolve structural issues in a more cost-effective and timely manner leading to dramatic reductions in the total life-time cost of ownership of a naval vessel.

Researchers have begun to investigate the development of structural health monitoring (SHM) systems for high-performance ships (Farrar, *et al.* 2009). Any SHM system designed and deployed for aluminum hull ships must exhibit the ability to detect the onset of fatigue in the hull components. This project explores data-driven algorithms that can be autonomously executed by the hull monitoring system to identify fatigue damage. Known hull hot-spots (e.g., base plates, heat affected zones near welds) are often instrumented with strain gages to record the hull response under cyclic wave loading (Bachman, *et al.* 2007). The strain gages would normally be interfaced to a wired hull monitoring system. However, in recent years, wireless telemetry has been explored in the shipboard environment because of their potential to eliminate monitoring system wires (Lynch, *et al.* 2009). The reported benefits of wireless hull monitoring include lower installation costs and the installation of a larger number of sensors in the hull. Regardless of the type of hull monitoring system employed (e.g., wired or wireless), a scalable approach to processing hull response data for an accurate assessment of the hull health is still lacking. Until such algorithms are shown accurate and reliable in the detection of hull deterioration, acceptance of SHM in the naval engineering community will be limited.

## 2. Technical Objectives

This project explores data-driven algorithms that can be autonomously executed by the hull monitoring system to specifically identify fatigue damage. The approach to fatigue analysis depends on use of hull strain time history data to automate the process of damage detection. Time- and frequency-domain algorithms are adopted to continuously and autonomously count strain peaks in the recorded strain time histories. Using peak amplitude strains ( $S$ ) and the

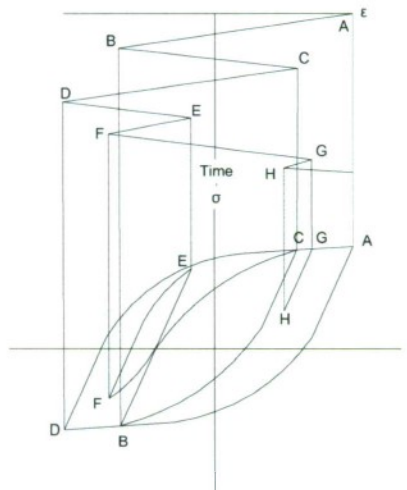


Figure 1: Rainflow cycle analysis via closed loop identification

accumulated number of peaks ( $N$ ), the Palmgren–Miner rule and the appropriate S-N curve for the ship’s aluminum alloy are selected to roughly track the fatigue life of the instrumented hull detail. The selection of these methods of tracking the fatigue life of hull components is motivated by their computational simplicity. In particular, these fatigue estimation algorithms are embedded into the computational cores of *Narada* wireless sensor nodes; *Narada* has been previously validated for hull monitoring on the FSF-1 SeaFighter (Lynch, *et al.* 2009).

The specific project objectives are:

- Rain flow assessment of strain time histories will be implemented along with Miner’s rule in the computational core of a wireless sensor for fatigue monitoring of aluminum components. Experimental validation will be performed on aluminum coupon specimens loaded under uniaxial load.
- Spectral methods to peak extraction will also be implemented with Miner’s rule in the computational cores of a wireless sensor. Again, experimental validation will be conducted using aluminum coupons loaded under uniaxial load.
- Third, the embedded fatigue analysis will be validated experimentally on complex aluminum hull connections at NSWC-Carderock.

### 3. Theoretical Background and Algorithms

#### 3.1 Rain Flow Peak Extraction and Miner’s Rule for Fatigue Estimation

Fatigue life monitoring begins by identifying cycles within a complex load time history. A number of cycle counting methods are used to reduce irregular load histories into a collection of constant amplitude events such as rainflow counting (primarily used herein), range-pair counting, and racetrack counting. Rainflow cycle counting has shown to be among the superior methods for cycle counting of irregular loads. In the rainflow method, cycles are identified in a manner in which closed hysteresis loops are identified from the stress–strain response of a material subject to cyclic loading. As shown in Fig. 1, closed hysteresis loops can be identified from the strain-

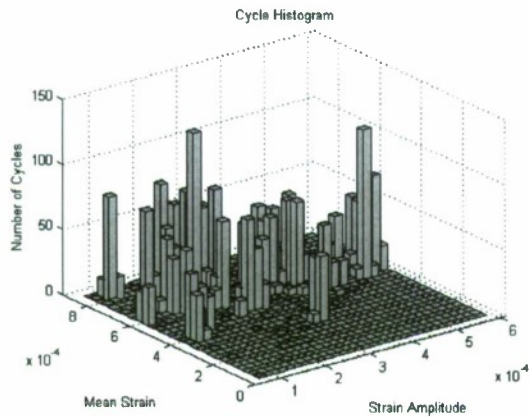


Figure 2: Histogram of cycle accumulation

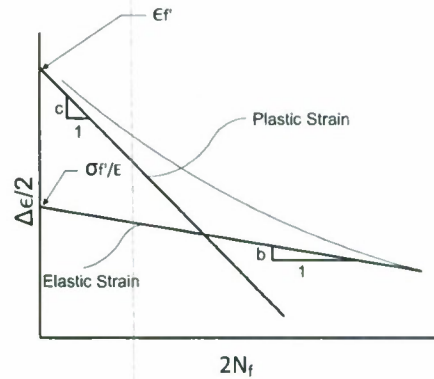


Figure 3: Strain-life curve

time history shown. Ranges A-D, B-C, E-F, and G-H, would represent cycles counted under rainflow counting techniques. Rainflow counting, however, is originally intended to be carried out once the entire strain history is known, since counting starts and ends at the maximum peak or valley. Due to the limited memory available in wireless sensors, it is not possible to wait until the entire load history has been realized before fatigue accumulation can be calculated. Rather, the ‘one-pass’ rainflow counting algorithm can be alternatively used since it does not require the full time history record. This method, which was used for embedment in this study, is a vector-based counting algorithm first demonstrated by Downing, *et al.* (1976) and later modified by Okamura, *et al.* (1979) to account for half cycles. The embedded rainflow counting algorithm starts by arranging sampled strain time history measurements into a single vector. From the set of strain data, peak and valley points inherent in cyclic measurements are identified and stored. The typical rainflow counting procedure is then performed on the set of peaks and valleys, identifying closed hysteresis loops and logging those ranges as cycles. For each cycle, both the strain amplitude and mean strain are recorded. This rainflow counting procedure identifies the same cycles as the traditional rainflow procedure that uses the entire strain time history. This fact makes the ‘one-pass’ rainflow counting procedure very attractive for continuous real-time monitoring of fatigue life using wireless sensors.

The ‘one-pass’ rainflow counting technique can be operated in a real-time manner for continuous monitoring of fatigue life. The compression of a strain time history from sampled points to cycles though, is not enough to monitor fatigue in the long-term. Further data compression is realized by accumulating identified cycles of mean and amplitude into a histogram similar to the one shown in Fig. 2. A fixed size histogram allows for *a priori* allocation of the available memory integrated with the wireless sensor, allowing for the near perpetual accumulation of fatigue cycles and thus continuous “real-time” fatigue life monitoring. Considerations of bin sizing in the mean and amplitude axes will be of importance in terms of mean and amplitude accuracy, as well as in terms of the scarce memory consumed.

Strain-life methods which account for mean strain effects are used in this project to predict fatigue life. First, the total strain amplitude can be expressed as the sum of an elastic strain amplitude and a plastic strain amplitude, each represented linearly against cycles to failure on a

log-log plot. Total strain amplitude versus cycles to failure,  $N_f$ , before mean stress (or mean strain) correction is written as:

$$\frac{\Delta\epsilon}{2} = \frac{\sigma_f'}{E} (2N_f)^b + \epsilon_f' (2N_f)^c \quad (1)$$

where:

- $\frac{\Delta\epsilon}{2}$  = strain amplitude
- $\sigma_f'$  = fatigue strength coefficient
- $E$  = modulus of elasticity
- $2N_f$  = reversals to failure
- $\epsilon_f'$  = fatigue ductility coefficient
- $b$  = fatigue strength exponent
- $c$  = fatigue ductility exponent

The constants  $b$  and  $c$  represent the slopes of the elastic and plastic strain. Similarly,  $\frac{\sigma_f'}{E}$  and  $\epsilon_f'$  are the y-axis intercepts of the elastic and plastic strain curves in Fig. 3. Eq. (1) is applicable if dealing with full cycles with zero mean strain. However, several researchers have proposed modifications to the strain-life relationship of Eq. (1) to account for mean stress effects including Morrow (1968) and Manson and Halford (1981). These relations all have their own advantages, but require the mean stress in order to evaluate the number of cycles to failure. A modification to the strain-life relation using mean strain instead of mean stress would be better because strain is measured and not stress. The need to track stress-strain around a hysteresis curve to determine mean stress is taken out of the picture, making the embedded process easier to implement. One such empirical relationship between total strain range,  $\Delta\epsilon$  and cycles to failure is adopted here. This empirical relationship which accounts for mean strain instead of mean stress is written as:

$$\Delta\epsilon = \frac{2(1-R)\epsilon_f'}{[(4N_f - 1)(1-R)^a + (2)^a]^{1/a}} \quad (2)$$

where:

- $R = \epsilon_{min}/\epsilon_{max}$  if  $|\epsilon_{max}| \geq |\epsilon_{min}|$
- $R = \epsilon_{max}/\epsilon_{min}$  if  $|\epsilon_{max}| < |\epsilon_{min}|$
- $\Delta\epsilon = \epsilon_{max} - \epsilon_{min}$

Here,  $a$  is equal to  $-1/c$ . The fatigue ductility coefficient,  $\epsilon_f'$ , fatigue strength exponent,  $b$ , and fatigue ductility exponent,  $c$ , determined for the strain-life relationship are used both directly and in computing the material constant,  $a$ . These parameters are best evaluated by performing cyclic testing in the laboratory. When fatigue data is not available or easily obtained, these parameters can be estimated from static properties or by using other estimation methods.

In this study, the empirical fatigue law of Eq. (2) will be used. To estimate the model parameters (fatigue ductility coefficient,  $\epsilon_f'$ , fatigue ductility exponent,  $c$ , and fatigue strength exponent,  $b$ ), the uniform material law by Bäumel and Seeger (1990) is used. For aluminum and titanium alloys, the strain-life equation is estimated as

$$\frac{\Delta\epsilon}{2} = 1.67 \frac{\sigma_b'}{E} (2N_f)^{-0.95} + 0.35(2N_f)^{-0.69} \quad (3)$$

where:  $\sigma_b$  = yield stress.

While Eq. (3) will not be used, one can however extract the fatigue ductility coefficient,  $\epsilon_f'$ , fatigue ductility exponent,  $c$ , and fatigue strength exponent,  $b$  from it. With knowledge of these constants, the material constant,  $a$ , can be estimated and Eq. (2) can be written in its final form as:

$$\Delta\epsilon = \frac{2(1-R)0.35}{[(4N_f - 1)(1-R)^{-0.4} + (2)^{-0.4}]^{1/-0.4}} \quad (4)$$

In this form, the mean strains and strain amplitudes obtained through rainflow counting are sufficient for determining the fatigue life,  $N_f$ , of an instrumented component. Although it is possible to embed a mean stress procedure, it will require more work for the wireless sensor and may be unnecessary as the prediction proposed in Eq. (4) has been shown to compare extremely well with data received from alloys tested under a variety of different tensile and compressive mean strains (Collins 1981).

The fatigue life corresponding to each cycle is an indication of the amount of damage imposed on the material due to that specific cycle. In this way, one can start to accumulate and monitor damage. The damage summation of each cycle is done using the Palmgren-Miner linear damage hypothesis originally proposed by Palmgren (1924) and later modified by Miner (1945). The Palmgren-Miner rule is written as:

$$D = \sum_{i=1}^k \frac{n_i}{N_i} \quad (5)$$

where:  $D$  = accumulated damage  
 $k$  = total number of cycles in a loading spectrum  
 $i = i_{th}$  applied stress/strain level  
 $n_i$  = number of cycles at stress/strain level  $i$   
 $N_i$  = fatigue life at stress/strain level  $i$

This method implies that failure occurs when the summation of cycle ratios,  $n_i/N_i$ , is equal to 1. It should be noted that by using strain-life methods, the initial cracking is predicted instead of complete failure. Further monitoring of fatigue damage (*i.e.*, after the initiation of cracking) requires crack propagation methods which are beyond the scope of this project.

The value residing in each bin of the accumulated cycle histogram represents the number of cycles at a specific strain amplitude and mean. The position of each bin determines the fatigue life of that particular bin, since it represents the strain amplitude and mean strain required for the strain-life relation. In the embedded implementation, cycles incurring damage below a specified threshold result in their elimination from the analysis. Signal noise will generate high amounts of low amplitude cycles, which when accumulated over an excessive amount of time may falsely contribute to the expended life of the material. Although certain materials have no defined fatigue limit, this liberty is assumed safe as noise level amplitudes are far below reasonably

assumed estimations for fatigue limits of these materials. It is important to use damage as the parameter for which cycles are counted or eliminated from analysis. Very small amplitude cycles at very high mean stress may result in relevant fatigue damage, and should not be eliminated from analysis.

### 3.2 Spectral Methods for Fatigue Estimation

A frequency domain approach to cycle identification for estimation of fatigue accumulation is also explored as an alternative to the proposed rainflow methods. Since many loading environments arise as stochastic processes (e.g., live loads, wind, waves), it is appropriate to use power spectral density (PSD) as a statistical function describing operational loads. The main motivation for the frequency domain approach is to use only a few statistical parameters deduced from a power spectrum to estimate fatigue life rather than doing continuous cycle counting in the time domain as is the case in rainflow counting methods. Many results exist for the case of narrow band stationary and ergodic random signals, especially those having a Rayleigh stress range distribution; however, one would like to have a procedure capable of handling wide band loading as well (Kirkby 1966). The Dirlik (1985) approach used here provides a closed form expression linking any given power spectral density to a probability density function of rainflow ranges when the random process is stationary and ergodic. The Dirlik procedure uses a Monte Carlo approach to generate stress time histories from various PSD shapes. Time domain rainflow counting is performed and a probability density function of rainflow ranges is linked to the corresponding PSD shape. Dirlik's solution is empirically derived by fitting rainflow range distributions to simulated data and is technically restricted to Gaussian processes. Theoretically based solutions exist under certain conditions, (e.g., Bishop and Sherratt (1990)) but Dirlik's method remains among the most frequently employed techniques due to its simplicity and due to its sufficient level of accuracy under required conditions.

The bulk of signal processing in Dirlik's method lies in the Fourier transform used to convert time-history strain data to the frequency-domain. A fast Fourier transform (FFT) is used to determine the power spectral density (PSD) function of strain data collected. The PSD is the base of all calculations in the analytical procedure. Specifically of interest are the spectral moments, where the  $n^{th}$  moment is defined as:

$$m_n = \frac{1}{\pi} \int_0^{\infty} \omega^n G(\omega) d\omega \quad (6)$$

or, in the case of a discrete PSD, can be visually observed in Fig.4 and written as

$$m_n = \sum_{f=0}^{f_{max}} f^n G(f) df \quad (7)$$

Many probabilistic characteristics of the signal arise from these moments. In 1945, Rice (1945) provided the relationship for the number of upward zero crossings and peaks per second based solely on spectral moments, paving the way for a fatigue life estimation based on power spectral density. The relations are seen below as:

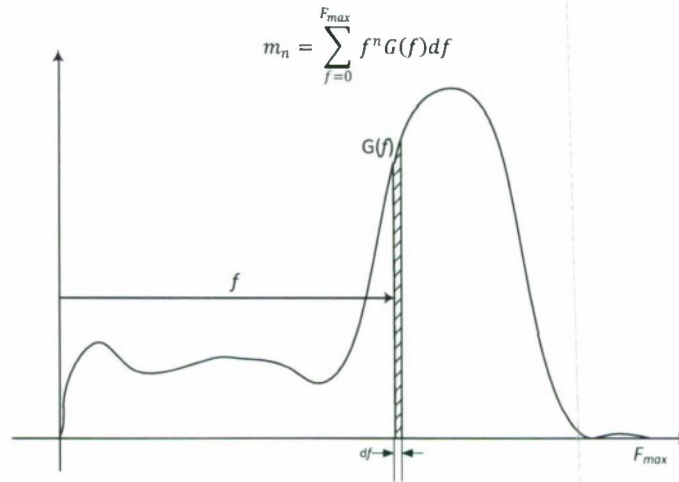


Figure 4: Spectral moments of the strain/stress PDF

Expected number of zero crossings per unit time,  $\lambda_0$ :

$$\lambda_0 = \sqrt{\frac{m_2}{m_0}} \quad (8)$$

Expected number of peaks per unit time,  $\mu$ :

$$\mu = \sqrt{\frac{m_4}{m_2}} \quad (9)$$

Irregularity factor,  $\gamma$ :

$$\gamma = \frac{\lambda_0}{\mu} = \sqrt{\frac{m_2^2}{m_0 m_4}} \quad (10)$$

Irregularity factor is the measure of the expected ratio of zero-crossings to peaks, approaching zero for the wide band case and one for the narrow band case. Other important characteristics arising from the spectral moments include the root mean square (RMS),  $\sigma_x$ :

$$\sigma_x = \sqrt{m_0} \quad (11)$$

and mean frequency,  $X_m$ :

$$X_m = \frac{m_1}{m_0} \sqrt{\frac{m_2}{m_4}} \quad (12)$$

From the above variables, Dirlik's rainflow – range probability density function,  $P_{RR}$ , is given as:

$$P_{RR}(z) = c_1 \frac{1}{\tau} e^{-z/\tau} + c_2 \frac{z}{\alpha^2} e^{-z^2/2\alpha^2} + c_3 z e^{-z^2/2} \quad (13)$$

where:

$$z = \frac{x}{2\sigma_x} \quad (14)$$

$$c_1 = \frac{2(x_m - \gamma^2)}{1 + \gamma^2} \quad (15)$$

$$\alpha = \frac{\gamma - x_m - c_1^2}{1 - \gamma - c_1 + c_1^2} \quad (16)$$

$$c_2 = \frac{1 - \gamma - c_1 + c_1^2}{1 - \alpha} \quad (17)$$

$$c_3 = 1 - c_1 - c_2 \quad (18)$$

$$\tau = \frac{1.25(\gamma - c_3 - c_2)}{c_1} \quad (19)$$

The probability density function of rainflow ranges relates fatigue life to a measured power spectral density. Expected damage can be calculated for any kind of S-N relation by the expected damage per unit time,  $E(D)$ :

$$E(D) = \mu \int_0^{\infty} \frac{1}{N(S)} P_{RR}(S) dS \quad (20)$$

where  $N(S)$  is the number of cycles to failure for a stress range  $S$ . In the case of a straight line log-log scale representation of the S-N curve, the following can be used:

$$N(S) = \frac{K}{S^b} \quad (21)$$

where  $K$  and  $b$  are material constants. Substituting Eq. (21) into Eq. (20) for the total damage expected from time  $t=0$  to  $T$ , the following is obtained:

$$E(D)_T = TK^{-1}\mu \int_0^{\infty} S^b P_{RR}(S) dS \quad (22)$$

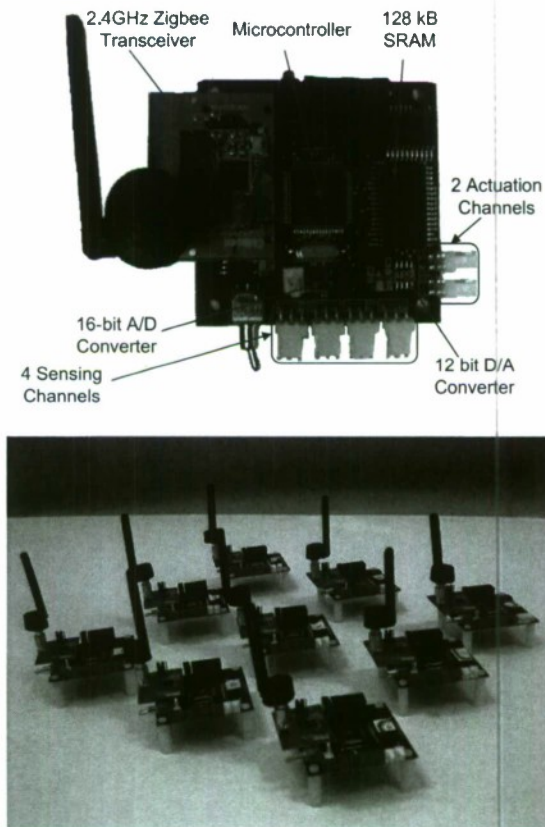


Figure 5: *Narada* wireless sensing node: (top) key components highlighted; (bottom) small network of nodes ready for deployment.

#### 4. Experimental Validation of the Embedded Fatigue Estimation Algorithms

##### 4.1 Implementation in the *Narada* Wireless Sensor Node:

The aforementioned fatigue estimation algorithms were selected for embedment in the computational core of the *Narada* wireless sensor node. This particular wireless sensor node has been previously validated during sea trials of the FSF-1 SeaFighter LCS (Lynch, *et al.* 2009). The *Narada* wireless sensing unit shown in Fig. 5 was developed at the University of Michigan. The *Narada* uses an Atmel Atmega128 microprocessor with 128kB of external SRAM for data storage and computation. The external memory allows the unit to store up to 64,000 data points at one time. Wireless communication is realized via a Chipeon CC2420 IEEE802.15.4-compliant wireless radio, making the unit exceedingly versatile for developing large, scalable wireless sensor networks. This unit utilizes a four channel, 16-bit Texas Instruments ADS8341 ADC for data acquisition, and a two channel, 12-bit Texas Instruments DAC7612 digital-to-analog converter (DAC) for actuation capability.

The embedded rainflow fatigue estimation procedure utilizes the 128kB of external SRAM on the *Narada* wireless sensor node. The external memory bank is divided into two 64kB halves

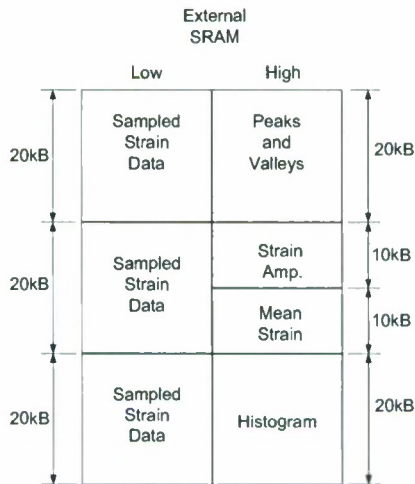


**Figure 6: Memory map for rainflow-based fatigue monitoring procedure**

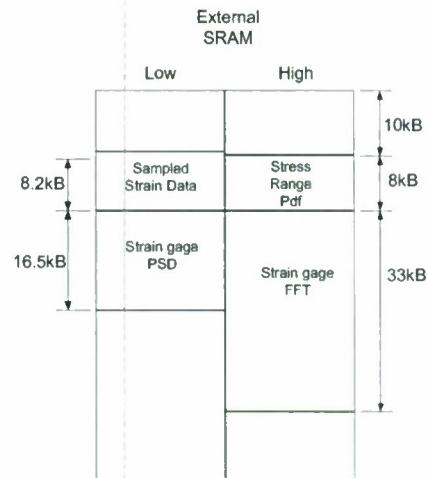


**Figure 7: Memory map for embedded Dirlik fatigue monitoring procedure**

denoted as low and high (Fig. 6). In the rain flow implementation, strain data acquired is stored on the low side in three separate blocks with a capacity of nearly 20kB each. This allows for the acquisition and processing of data sets containing nearly 10,000 data points of 2-bytes (or 16-bits). The three stage data acquisition guarantees the continuous acquisition of strain data in one block while fatigue life procedures are performed simultaneously on a previously attained set of strain data. After a stack of memory is filled, a peak picking algorithm is performed on the set of strain data. A set of only peaks and valleys are stored in a specific location on the high side of the external SRAM. The extreme condition considered for sizing memory allocation occurs when all points acquired during sampling result in peaks or valleys of the strain response signal, requiring an equally sized 20kB memory allocation. The rainflow counting procedure is carried out on the set of peaks and valleys and stored on the high side of the external SRAM. Extreme conditions here would see less than half the number of peak/valley points as the maximum number of cycles, requiring 10kB of memory allocation for strain amplitude and mean strain each. The remaining 20kB of external SRAM on the high side is used as a continuously updated histogram. In the case where the number of cycles is represented as a 2-byte integer, 10,000 unique strain amplitude-mean strain combinations are available. Any  $m$ -by- $n$  product of amplitude bins,  $m$ , by mean bins,  $n$ , less than 10,000 are admissible. In this project, cycles are accumulated in a 2-byte memory slot, limiting the maximum number of cycles that can be accumulated for a specific strain amplitude and mean strain to 65,535 cycles. All processing procedures carried out on the high side of the external SRAM allow for continuous strain gage data acquisition on the low side by way of an interrupt on the analog-to-digital converter. The external SRAM layout for the rainflow method is summarized in Fig. 6.

The embedded spectral-based fatigue estimation is also embedded into the *Narada* wireless node external memory (Fig. 7). Again, the memory map is laid out into two 64kB halves. A maximum of 32,000 2-byte strain gage samples can be collected at one time but the FFT computation restricts us to 4096 samples as implemented on *Narada*; hence, 8.2 kB is allocated for sampled strain data storage. Once the FFT algorithm is run with the sampled data, a complex

**Table 1: Analysis of communication requirements of centralized and proposed decentralized fatigue life monitoring methods**

Methods	Transmission payload byte
Centralized <i>Rainflow counting performed on central server after all time history data is received</i>	$N_{data} * 2 \text{ byte}$ $= 30000 * 2 = 60 \text{ kbyte}$
Decentralized <i>Rainflow counting conducted on wireless sensing nodes with cycle histogram sent to server</i>	$Histo * 2 \text{ byte}$ $= 10000 * 2 = 20 \text{ kbyte}$
<b>Transmission reduction = ~ 67 %</b>	

Note: Time history data length,  $N_{data} = 30000$  points  
Histogram size,  $Histo = 10000$  bins

floating point number is stored for each point resulting in 33 kB of FFT data. The subsequent PSD calculation requires half the data sizes as the floating point numbers are real only. The stress range PDF is given a size of 2,000 points, ranging from 0 to 20 ksi. It is up to the user and available memory as to how resolute the stress range PDF should be. The sampled strain data and corresponding PSD are stored in the lower half of memory while the stress range PDF and strain FFT are stored in the higher half as shown in Fig. 7.

By embedding the fatigue life monitoring process into *Narada*, great savings in communication can be realized. Table 1 shows an analysis of communication requirements of a centralized counting implementation and a decentralized computing implementation. The example in Table 1 is consistent with 10 minutes of continuous data acquisition at a sampling frequency of 50 Hz. The decentralized implementation sends one histogram at the end of the ten minutes. A transmission reduction of approximately 67% is the result of a ten minute experiment. Fatigue life monitoring though, will require much longer periods of data acquisition and will further exploit this transmission reduction.

Fig. 8 shows the transmission payload over a 5 hour period for both the centralized

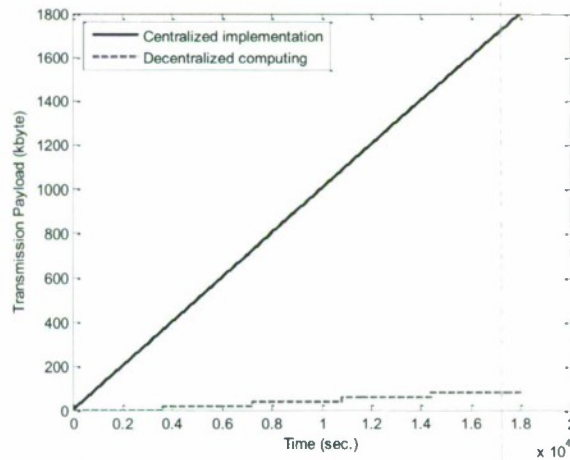


**Figure 8 : Comparison of decentralized and centralized computing communication costs**

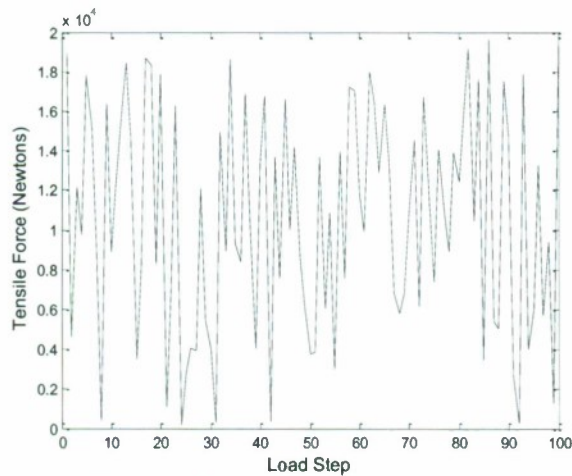


Figure 9: Sample random amplitude load

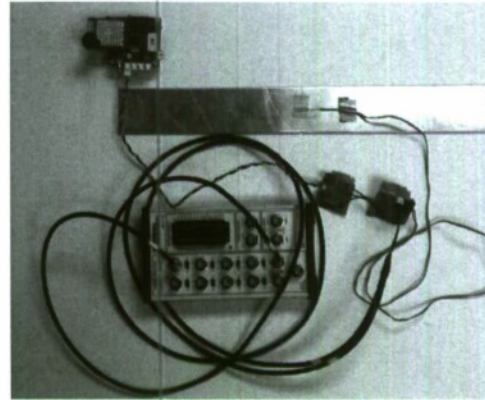


Figure 10: Dual data acquisition of strain gage

implementation (where raw data is continuously streamed over the wireless channel) and the decentralized implementation (where fatigue histograms are locally updated and occasionally transmitted). Raw strain gage data increases as a linear function of time for any given sampling frequency in the centralized implementation. The number of unique strain amplitude and mean strain cycles sent by the histogram in the decentralized implementation remain fixed, and thus increase by the same amount at each request. Histograms are sent once each hour. At the end of the 5 hour example, the decentralized computation produces 1700 less kilobytes for transmission than the centralized implementation, resulting in a 94% transmission reduction. Further increases in time between histogram transmissions will result in even greater transmission savings. By receiving compact amounts of meaningful data transmitted upon request as opposed to receiving vast amounts of unprocessed data transmitted frequently, faster and more efficient analysis of the structural member under observation can be conducted.

#### 4.2 Aluminum Bar Specimens under Uniaxial Tensile Loading:

For this study, a simple specimen constructed of 6061-T6 aluminum alloy is used. The specimens are 1/8 in thick bars roughly 17 in long and 3 in wide. A 10 mm (0.4 in) strain gage is used (Tokyo Sokki Kenkyujo Co., Ltd. TML PFL-10-11-1L 120 $\Omega$ ) at the mid-section of the bar. Bonding areas are removed of grease and oils and lightly polished before adhering strain gages. Fatigue loading is applied using an MTS Series 318 electrohydraulic closed loop load unit. The load unit consists of two smooth vertical columns that are joined by two stiff cross members, one being fixed with an integrally mounted hydraulic actuator. Hydraulic grips hold the specimen in place during loading. A representative loading input is shown in Fig. 9 (this is a random amplitude loading).

In an effort to compare a wired fatigue analysis with the embedded analysis executed by the *Narada* wireless sensing node, the specimen strain gage is split with its output interfaced to both a wired and wireless systems as shown in Fig. 10. The strain gage lead wires are first attached to a Wheatstone bridge circuit to convert the gage resistance change into a voltage signal. The voltage output of the bridge circuit is first passed to the input of an op-amp amplification circuit before being passed on to the *Narada* wireless sensor node. The amplifier circuit amplifies the

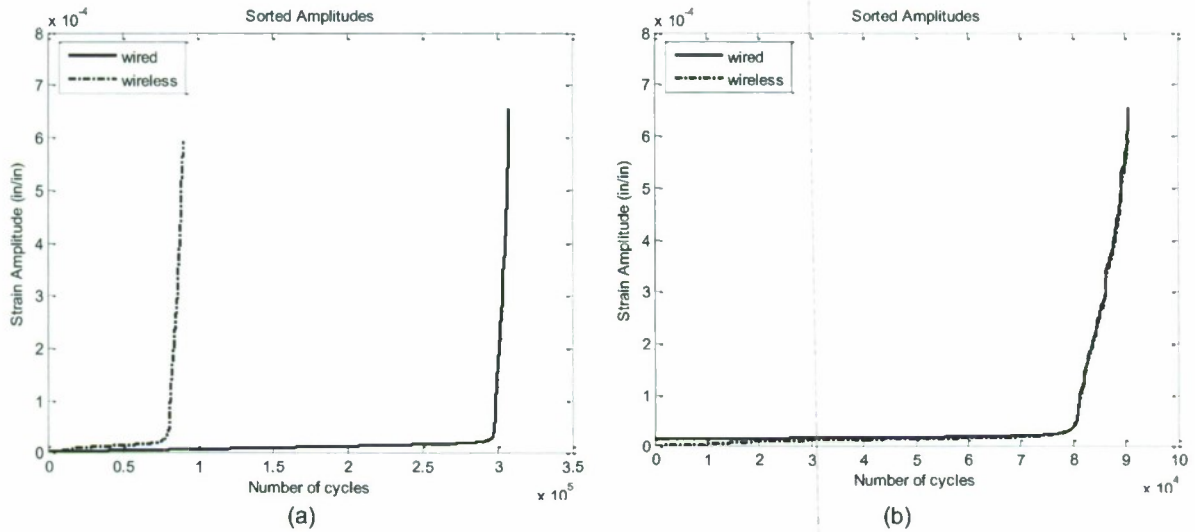


Figure 11: (a) Reordered amplitudes over entire time history (b) wired and wireless amplitude overlay

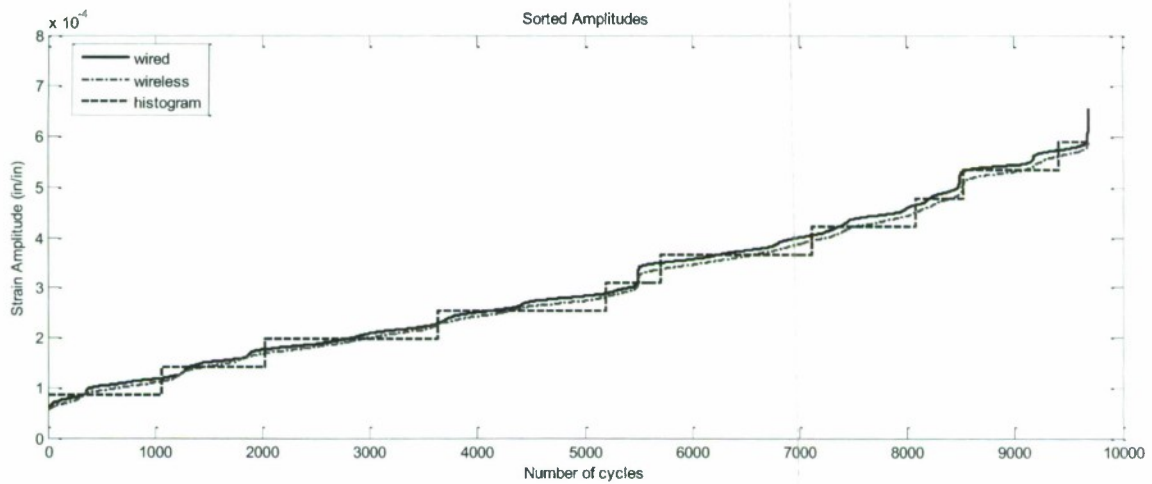
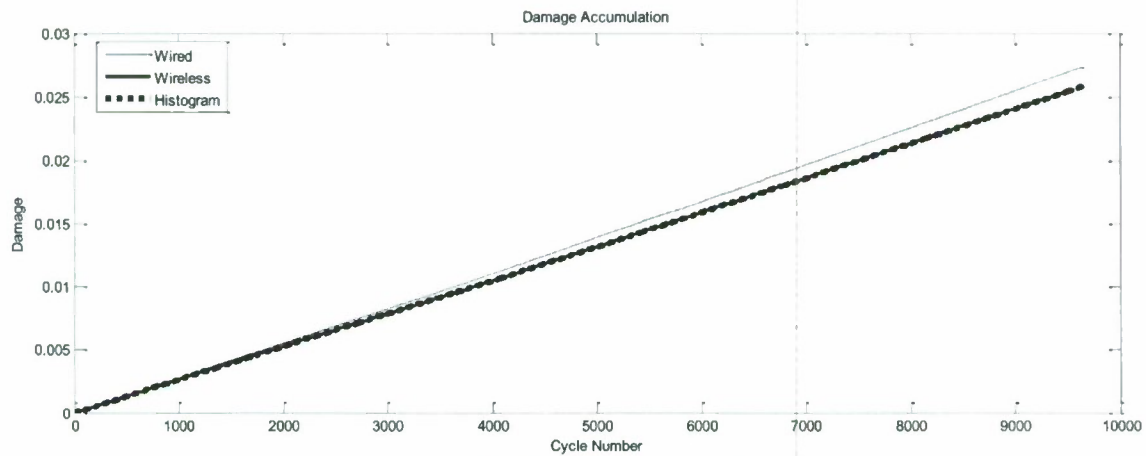


Figure 12: Close up view of relevant wired, wireless, and histogram cycle outputs

bridge voltage by a factor of 50. The output of the bridge circuit is also passed to a National Instruments BNC-2110 data acquisition system interfaced to a personal computer running LabView. The sampling rate used by the *Narada* mode is 50 Hz while that used by the National Instruments system is 100 Hz.

First, the embedded rainflow counting method is tested and validated. Specimens are subject to variable amplitude uniaxial tensile cyclic loading. The loading pattern consists of 100 randomly generated peaks and valleys as shown in Fig. 9. Load sets are looped continuously during testing until the end of the test. To make a comparison between the wired and wireless fatigue monitoring system, the wireless sensing system is set to transmit all cycles, giving strain amplitude and mean strain for each cycle at the end of each sampling block. Stress peak and mean histograms are transmitted periodically during testing upon user request. Fig. 11a compares wired and wireless rainflow cycle counting amplitudes, plotting all amplitudes



**Figure 13: Damage accumulation**

**Table 2: Fatigue Life Results**

	Total Cycles	Cumulative Damage	% difference
Wired	9642	.00273	-----
Wireless	9570	.00256	6.22
Binned Wireless	9684	.00259	5.13

calculated during rainflow counting, reordered lowest to highest. It can be seen that the wired system produces more low amplitude cycles than the wireless system. This can be explained as an effect of splitting the strain gage to the two independent DAQ systems, which introduce an increase in signal noise to the wired signal. Additionally, the wired DAQ system samples twice as fast as the wireless system resulting in more peaks and valleys to consider during rainflow counting. Figure 11b shows the amplitudes read from each system where the signal noise is removed from the wired strain data, resulting in a more accurate comparison of the two systems; similar amplitude outputs are extracted by both systems. Fig. 12 provides a closer look at the wired and wireless amplitudes that overlay in Fig. 11b. Fig. 12 also includes the results recorded in the histogram during testing. For the division of the histogram bins, 327 unique amplitudes and 21 unique mean values are selected. Damage accumulation for the three sets of results is shown in Fig. 13. Damage value represents the damage accumulated as calculated by the Palmgren-Miner method (namely, Eq. (5)). The maximum damage results in Fig. 13 are also listed in Table 2. Excellent agreement between the wired and wireless systems is found.

The Dirlik-based spectral fatigue damage estimation was also embedded in the *Narada* wireless sensor and validated. First, constant amplitude tests were run at various stress ranges in an effort to observe expected probability distributions. Probability density functions resulting from the embedded Dirlik procedure for constant amplitude testing at ranges 1-8 ksi are shown in Fig. 14. These tests are run to achieve a simple visual confirmation of the expected change in the distribution for various stress ranges. As would be expected, the area under the curve increases near the actual stress range for each individual test. To compare the embedded rainflow counting and embedded Dirlik procedures, the samples obtained from strain gage response of a laboratory fatigue specimen cycled under narrow band loading with an RMS stress range of 6 ksi is used.

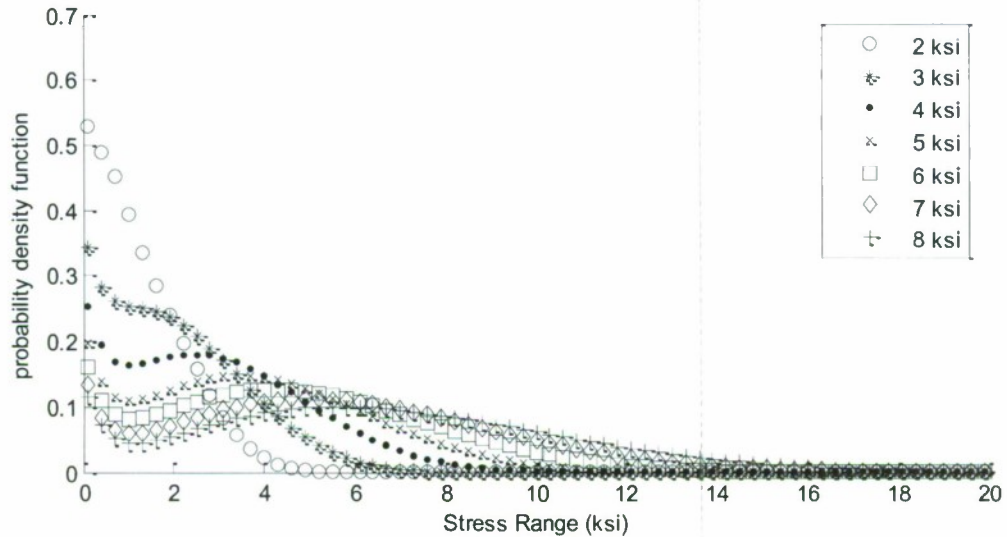


Figure 14: Probability distribution for varying stress ranges for an aluminum coupon

Table 3: Time and frequency domain number of cycles and expected damage

	Rainflow		Dirlik	
	N	D	E[N]	E[D]
Sample 1	5226	2.0754e-6	13852	1.4256e-6
Sample 2	5033	2.5871e-6	13485	1.0990e-6
Sample 3	5307	1.0109e-6	15649	1.3732e-6
Sample 4	4970	2.0767e-6	13672	1.8415e-6
Sample 5	4945	2.5781e-6	14437	7.7836e-7

Fig. 15 shows the (a) windowed time domain response and (b) PSD for a 100,000 point time history sampled at 100 Hz. Also shown are the corresponding stress range distributions via (c) rainflow counting in the time domain and (d) Dirlik procedure using spectral moments. The number of total cycles from the rainflow counting method and Dirlik method are shown in Table 3 along with the damage estimates from each method. The total number of cycles by rainflow counting is simply given by summing the number of cycles in each bin of the cycle histogram. For the spectral procedure, the expected number of cycles for a time  $T$  is given by:

$$E[N] = E[P] \cdot T \quad (23)$$

where  $E[P] = \mu =$  expected number of peaks per second.

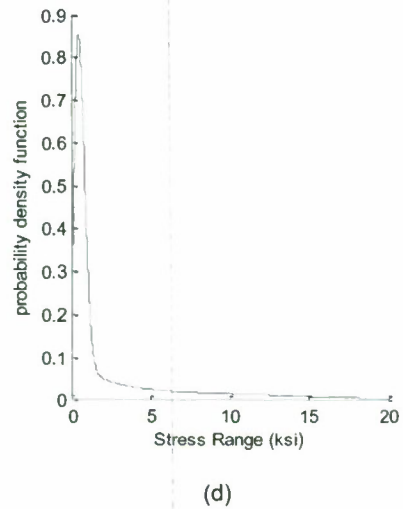
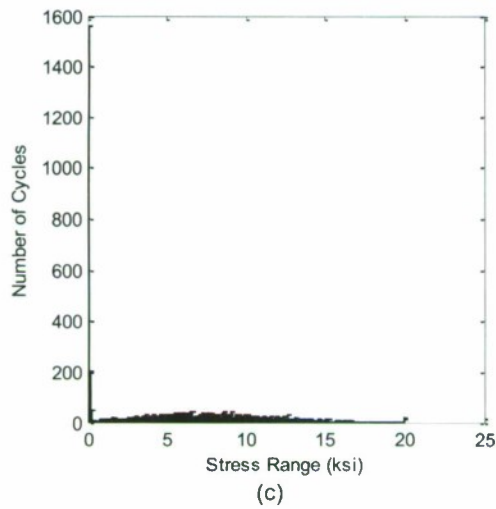
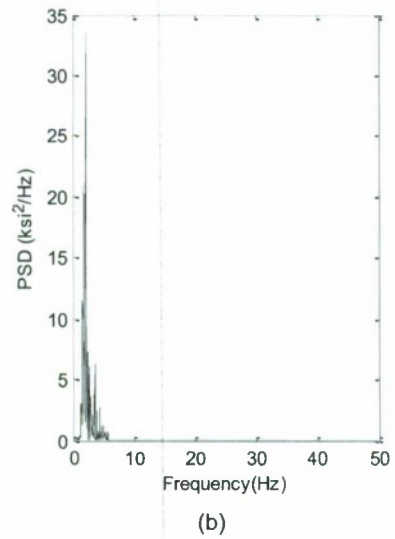
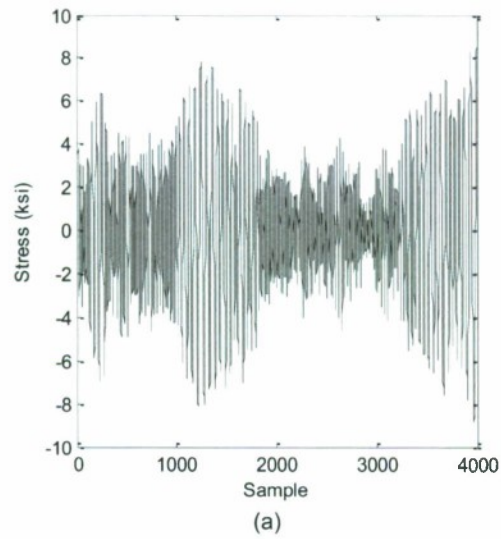


Figure 15: (a) Stress - time history of fatigue loading; (b) one-sided PSD; (c) rainflow counting algorithm; (d) Dirlik PDF of rainflow ranges.

#### 4.3 Validation on the Monitored Aluminum Hull Integrity (MAHI) Phase I Specimen:

The NSWCCD Monitored Aluminum Hull Integrity (MAHI) program presents an opportunity to further validate the embedded fatigue life estimation algorithms. The MAHI fatigue test program is specifically focused on the design, fabrication and fatigue testing of aluminum hull stiffened-plate structural specimens. In this project, the first phase specimen is tested which consists of a single stiffened plate element with an intersecting stiffened bulkhead element. The MAHI fatigue test specimen is shown in Fig. 16. The specimen consists of a 5083-H116 aluminum plate, a tee stiffener machined from an A16061-T6 aluminum wide-flange beam extrusion, and a bulkhead detail made from A15083-H116 plate, as well as a vertical tee stiffener on the bulkhead machined from the above 6061-T6 stock extrusion. The specimens were fabricated according to generally accepted shipyard practices so as to respond with typical crack initiation behavior.

Fatigue testing was performed in the NSWCCD Fatigue Testing Laboratory in Carderock, MD. The NSWCCD fatigue laboratory contains six uniaxial servo-hydraulically controlled load frames of varying capacity, all having full tension and compression cyclic loading capability. An Instron 220-kip machine was used in the experimental tests for this study. The Instron fatigue testing machine is computer-interfaced with analog controllers to allow for complex test loadings. The test machines are also equipped with wired data acquisition system with channels dedicated to recording applied load, displacement, and strain gage responses; the system is capable of sampling rates up to 50 kHz.

The stiffened plate specimen was subject to a zero mean random loading consisting of a computer-simulated sequence of 10,000 endpoints of Rayleigh distributed extrema generated using a first order auto-regressive technique. Endpoints are connected by haversine curves to produce a continuous waveform of unit RMS value. Loading is customized by multiplying each endpoint of the load sequence by the product of desired RMS stress and average cross sectional area of the specimen. Specifically, 3 ksi RMS loading was used in the tests reported in this study.

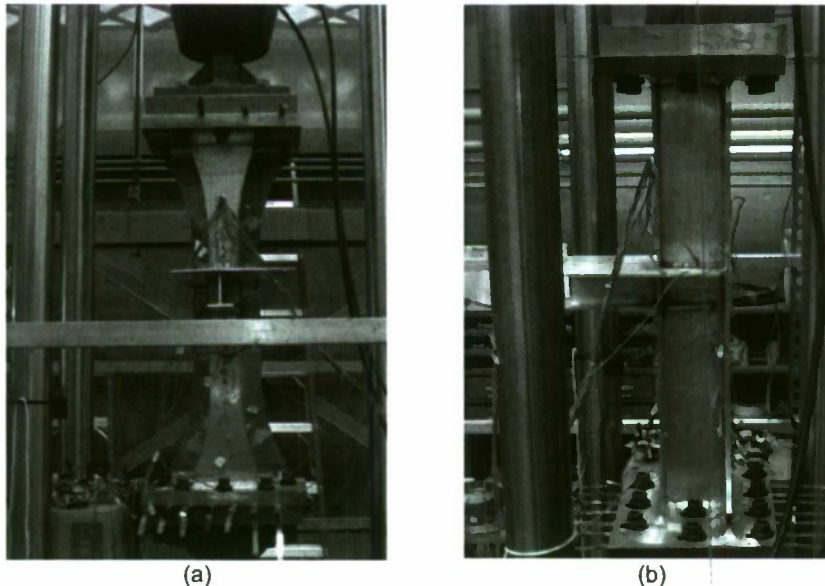


Figure 16: MAHI aluminum hull fatigue specimen: (a) front view; (b) side view

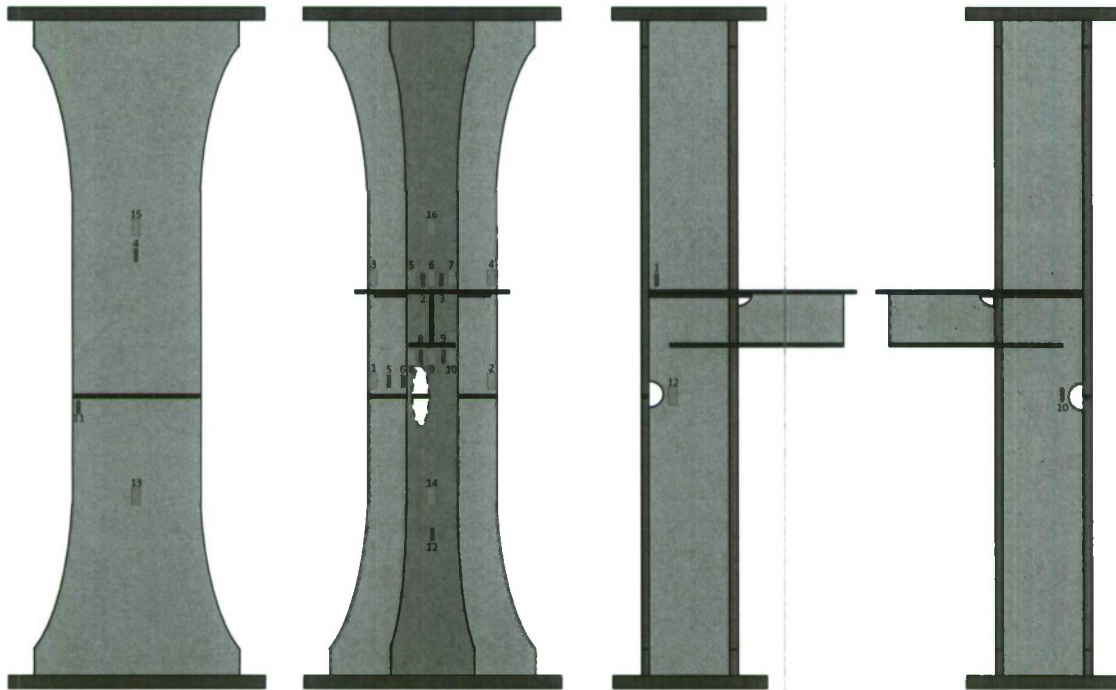
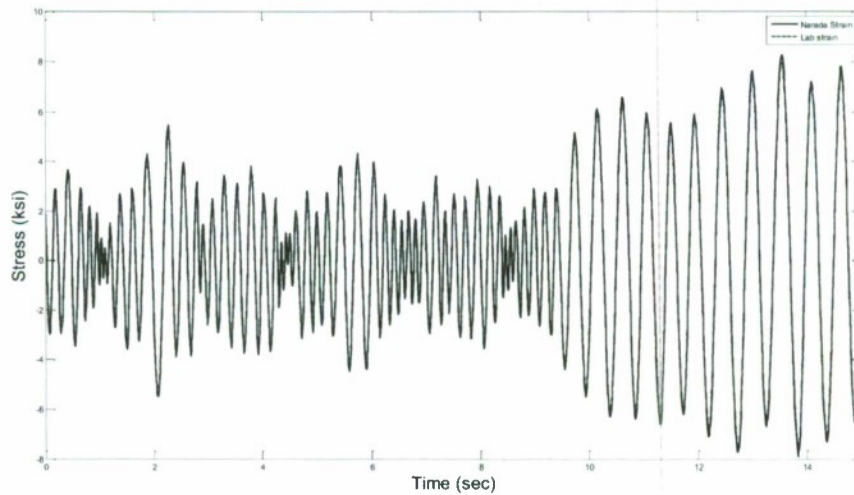


Figure 17: Strain gage installation on the MAHI aluminum stiffened hull fatigue specimen: (left) front/back view; (right) side/side view. Yellow gages are wired while the green gages are wireless.



Figure 18: (Left) strain gage installation on the MAHI specimen; (right) *Narada* wireless sensor nodes for data acquisition from the "green" strain gages.

All peaks are followed by an equal and opposite trough. All loading is performed under load control. The 10,000 point load sequence was continuously repeated 20 to 30 times during day time hours and rested at night. The stiffened plate specimen was axially loaded at a load rate of 400 to 500 kips per second. The laboratory data acquisition system collected strain gage response data at various locations on the aluminum hull specimen. An additional set of strain gages interfaced to the *Narada* wireless sensor node is also installed (many in locations redundant to the location of the wired strain gages). Fig. 17 provides a drawing of the test specimen with the installed strain gage sensor layout for both the *Narada* wireless system as well



**Figure 19: Data comparison between NSWCCD tethered system and *Narada* wireless system**

as for the laboratory data acquisition system. Fig. 18 documents the test setup. Several channels were dedicated to raw strain gage data acquisition as well as the embedded rainflow counting and Dirlik fatigue life monitoring procedures described in this report.

All *Narada* data acquisition is conducted at a sampling rate of 100 Hz. Raw strain data acquisition was performed continuously as well as the embedded rainflow counting (except when loading was suspended). Raw strain data was transmitted from the *Narada* to a receiver base station after 10,000 samples were collected (roughly every 100 seconds) and routed to a server (laptop) via a USB connection for long-term storage. Processed rainflow counting data was collected periodically for updates. Data for the embedded Dirlik procedure was collected for one minute duration every hour. Therefore, the resulting stress range PDF was applied to a one hour time period when calculating the accumulated damage. Processed data from the Dirlik procedure was also transmitted periodically. Efforts were made to sample the complete range of the 10,000 point load cycle so as to acquire all aspects of the load signal.

Results from strain gages corresponding to *Narada* wireless sensing unit channels and NSWCCD laboratory data acquisition channels are compared for raw strain gage response, rainflow counting histograms, and stress range PDFs. An effort is made to compare strain gages in areas assumed to experience similar stresses under uniaxial tension-compression. According to Fig. 17, one would expect *Narada* gage # 8 and NSWCCD gage # 8 to have similar strain gage responses. Fig. 19 shows that the *Narada* wireless sensing unit acquires accurate strain data needed for reliable fatigue life analysis. After collecting response data, the embedded fatigue algorithms are executed. In Fig. 20, histograms for the rainflow counting show the cycle extractions of *Narada* strain gage #6. For the purposes of comparison, this particular unit transmitted raw strain data as well as the embedded histogram periodically. Fig. 20(a) shows the histogram output from the embedded procedure after 4 days of continuous fatigue life processing while Fig. 20(b) shows the output from the rainflow counting on the raw strain gage data in post-processing. Final damage estimates compare well but poorly reflect indication of crack initiation due to the use of an arbitrary S-N curve in this study. Future NSWCCD laboratory research for this project

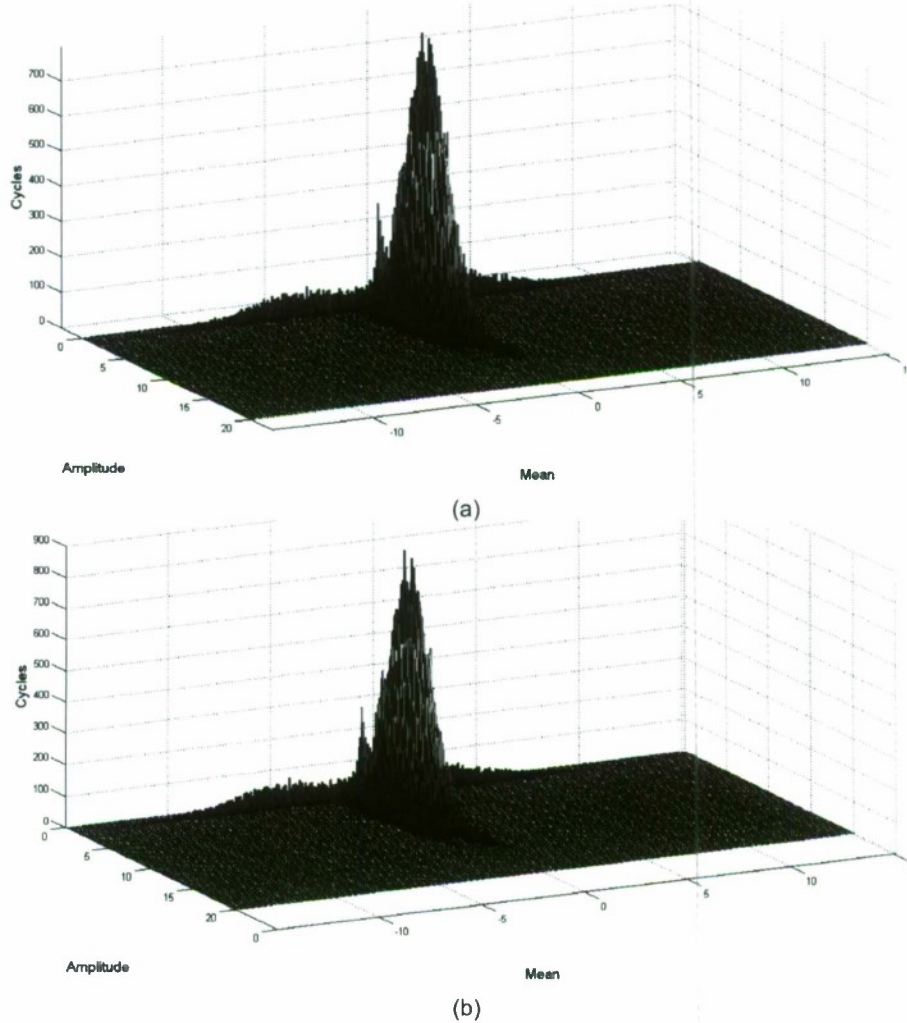


Figure 20: Rainflow counting histogram on Day 4: (a) embedded; (b) post processing

includes constructing system specific S-N curves so that final damage estimates would more accurately reflect crack initiation ( $D = 1$ ).

To validate the embedded Dirlik procedure, the stress range PDF produced by *Narada* strain gage #7 (calculated and stored on-board) is obtained and compared with raw strain data in post-process. Fig. 21 shows stress range PDFs generated at strain gage #7 with the one hour damage accumulation from each PDF. The comparison of the two embedded procedures (Fig. 20 and Fig. 21) along with the accuracy of the *Narada* wireless system against the tethered system (Fig. 19) displays the ability of the proposed decentralized fatigue life monitoring system to perform analyses typically reserved for central processing. Unfortunately, damage accumulation is difficult to compare as all strain gage channels were placed at unique positions on the specimen. However, damage accumulation for NSWCCD strain gage #9 and *Narada* strain gage #9 are shown in Fig. 22 because of their close proximity. Very similar damage accumulation can be observed for the two strain gages sensed on different networks and processed by centralized and decentralized systems.

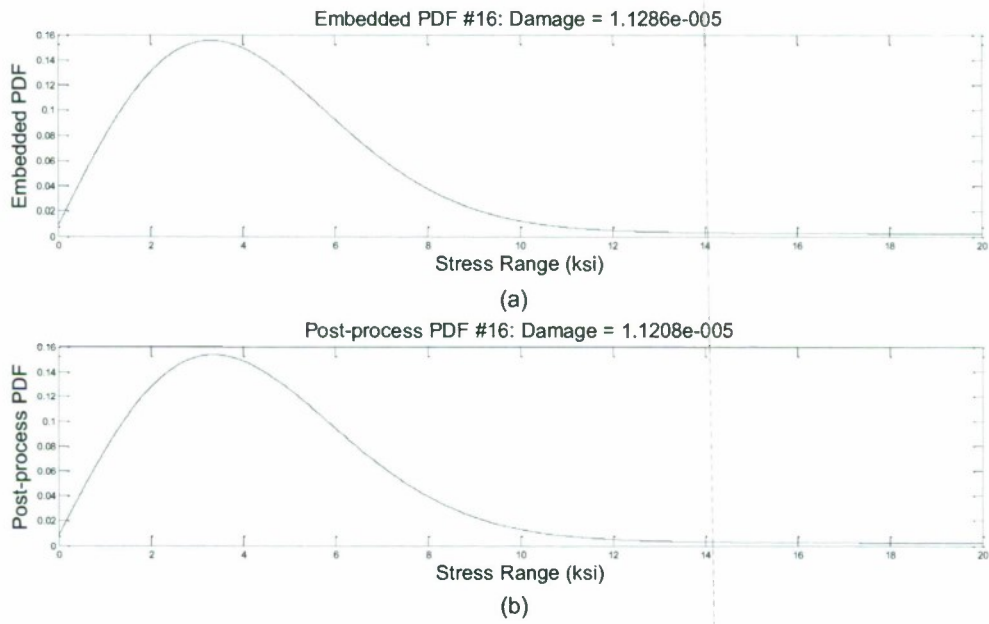


Figure 21: Stress range PDF obtained by the Dirlik formula: (a) embedded procedure; (b) raw data in post processing.

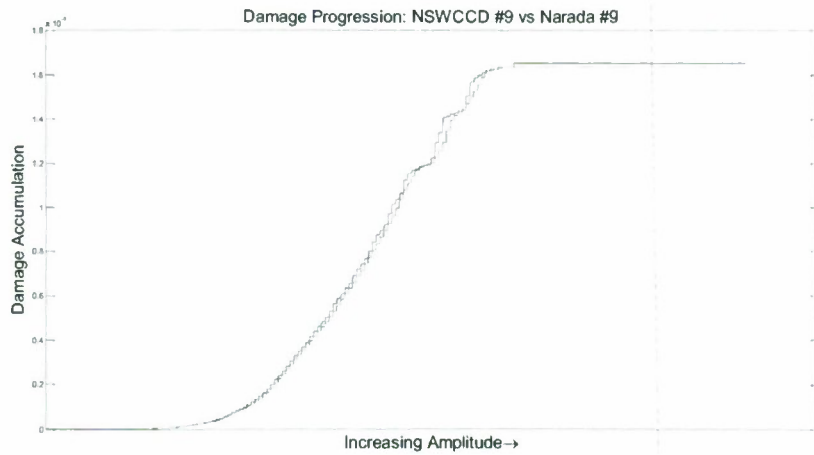


Figure 22: Damage accumulation for two closely situated strain gage sensors (NSWCCD #9 & Narada #9)

## 5. Summary and Future Work

This report describes a major effort towards the embedment of damage detection algorithms into the computational cores of wireless sensors for automate data interrogation in a wireless hull monitoring system. The advantages of embedded data processing include the preservation of wireless node power and the ability to deploy larger number of strain gages in a hull without concern of data inundation issues. Presented are two decentralized fatigue life monitoring schemes easily embedded and implemented in a wireless sensor network: rainflow peak and mean counting and the Dirlik spectral methods. The *Narada* wireless sensing node was shown to be accurate in its recorded time history data when compared to a traditional tethered data acquisition system. Furthermore, both the rainflow and Dirlik procedures were consistent and produced fatigue estimation consistent with one another. The ability of the *Narada* wireless system to accurately acquire data and then accurately process data provides us with the tool for decentralized processing in future wireless hull monitoring systems.

Current ship O&M strategies rely upon frequent visual inspection of ship hulls to determine damage. However, in the case of aluminum ships, this task is more difficult due to layers of fire installation installed in the hull. In addition, visual inspections of the entire hull are both costly and labor-intensive. Therefore, the installation of a structural health monitoring (SHM) system coupled with an effective damage detection methodology such as the approach presented in this report can reduce the cost of inspection by providing inspectors with a prioritized list of probable areas of damage. Our future investigation will extend the proposed fatigue estimation strategies to include reliability-based methods of estimating remaining life in a hull. In addition, inclusion of the fatigue estimates into a comprehensive life cycle analysis will be sought to dramatically reduce the total cost of ownership of the instrumented vessel.

## References

- Bachman, R.J., Woolaver, D.A., Powell, M.D. (2007), *Sea Fighter (FSF-1) Seakeeping Measurements*, Technical Report NSWCCD-50-TR-2007/010, Naval Surface Warfare Center Carderock Division, West Bethesda, MD.
- Bäumel, A., Seeger, T. (1990). *Materials Data for Cyclic Loading – Supplement 1*. Elsevier, Amsterdam.
- Bishop, N., Sherratt, F. (1990). “A theoretical solution for the estimation of “rainflow” ranges from power spectral density data.” *Fatigue & Fracture of Engineering Materials & Structures*, 13(4): 311-326.
- Collins, J.A. (1981). *Failure of Materials in Mechanical Design*. Wiley-Interscience, New York, NY.
- Dirlik, T. (1985). *Application of Computers in Fatigue Analysis*. PhD Thesis, University of Warwick, Coventry, UK.
- Downing, S., Galliard, D., Bereyni, T. (1976). “A Neuber's rule fatigue analysis procedure for use with a mobile computer” SAE Paper 760317, *SAE Automotive Engineering Congress*.
- Farrar, C., Park, G., Angel, M., Bemet, M., and Salvino, K. (2009). “Structural health monitoring for ship structures.” *Proceedings of the 7th International Workshop on Structural Health Monitoring*, Stanford, CA, pp. 1970-1977.
- Hess III, P.E. (2007). “Structural health monitoring for high-speed naval ships,” *Proceedings of the 6<sup>th</sup> International Workshop on Structural Health Monitoring*, Stanford, CA, pp. 3-15.
- Kirkby, W. (1966). *A Method of Fatigue Life Prediction using Data Obtained under Random Loading Conditions*. DTIC Document Number AD0642978.
- Lynch, J. P., Swartz, R. A., Zimmerman, A. T. (2009). *Seakeeping Trials of a Wireless Hull Monitoring System on the FSF-1 Sea Fighter*, Final Report, Grant N000178-04-D-4023-22, Office of Naval Research, Arlington, VA.
- Manson, S.S., Halford, G.R. (1981). “Practical implementation of the linear damage rule and damage curve approach for treating cumulative fatigue damage”, *International Journal of Fracture*, 17(2): 169-172.
- Miner, M.A. (1945). “Cumulative damage in fatigue”, *Journal of Applied Mechanics*, 12: A159-A164.
- Morrow, J. (1968). *Fatigue Design Handbook*. Advances in Engineering, Society of Automotive Engineers, Warrendale, Pa., pp. 21-29.
- Okamura, H., Sakai, S., Susuki, I. (1979). “Cumulative fatigue damage under random loads” *Fatigue Engineering of Materials and Structures*, 1(4): 409-419.
- Palmgren, A. (1924). “Durability of ball bearings”, *Z. Ver. dt. Ing.*, 68(14): 339-341.
- Rice, S.O. (1945). “Mathematical analysis of random noise,” *Bell Systems Technology Journal*, 24: 46-156.

Sielski, R. A. (2007). *Aluminum Structure Design and Fabrication Guide*. Ship Structure Committee Report SSC-452, United States Coast Guard, Washington, DC.

Tveiten, B. W., Wang, X., Berge, S. (2007). "Fatigue assessment of aluminum ship details by hot-spot stress approach," *Proceedings of the Society of Naval Architects and Marine Engineers*, Fort Lauderdale, FL.

THIS PAGE INTENTIONALLY LEFT BLANK